# Growth of Silicalite-1 by a Method Involving Separation of Reactants

Ester Mateo,[†] Ruth Lahoz,[‡] Germán F. de la Fuente,[‡] Andrés Paniagua,[§] Joaquín Coronas,*[,†,#] and Jesús Santamaría[†,#]

*Department of Chemical and Environmental Engineering, University of Zaragoza, 50018 Zaragoza, Spain, Nanoscience Institute of Aragon, University of Zaragoza, 50009 Zaragoza, Spain, Institute of Materials Science of Aragon, CSIC-University of Zaragoza, 50018 Zaragoza, Spain, and Department of Earth Sciences, University of Zaragoza, 50009 Zaragoza, Spain*

*Received September 27, 2006. Revised Manuscript Received November 16, 2006*

Two solutions of different concentration (that when mixed give rise to a common zeolite precursor gel) are separated by means of a laser-microperforated, 75 $\mu$m thick stainless steel sheet. During the hydrothermal synthesis, reactant diffusion from each side promotes crystallization of well-intergrown silicalite-1 crystals on each microperforation (ca. 80 $\mu$m in diameter). This method allows a micrometric control of the growth of the zeolitic material and has important advantages when compared with previous systems.

## Introduction

Zeolites are crystalline, hydrated aluminosilicates having microporous, regular structures. Zeolites have pores of molecular size that give them adsorption and catalytic[1] and ion exchange properties[2] of paramount importance in both the chemical industrial field and the study of new applications related to process intensification,[3] green chemistry,[4] hybrid materials,[5] medicine,[6] and so on. The ability to grow zeolites on porous supports can produce devices with very specific properties such as membranes,[7] membrane reactors,[8] microreactors,[9] reactive[10] and nonreactive gas sensors such as QCM[11] or zeolite-based capacitors,[12] corrosion protection coatings,[13] antimicrobial coatings,[14] zeolite-coated catalyst particles, and hollow zeolite particles.[16]

Commonly, a zeolite is prepared on a given support by either seeded or direct liquid-phase hydrothermal synthesis (LPHS), in which the porous support is immersed into the zeolite precursor solution and the membrane or film is synthesized under autogenous pressure. Alternatively, vapors containing amines and water can be employed to zeolitize silica or silica−alumina layers previously deposited onto a given surface.[17,18] In a previous work, silicalite-1 micromembranes were prepared by LPHS on laser-perforated, 75 $\mu$m thick stainless steel sheets.[19] The liquid-phase hydrothermal synthesis described above is the most widely used preparation method of synthesizing supported zeolites. This implies putting in contact the support with a solution usually having water, silicon and aluminum sources, sodium hydroxide, and a structure-directing agent (SDA). There are, however, significant problems with LPHS, mainly (i) the coexistence of nucleation (both in the bulk of the solution and in contact with the support) and growth of crystals, (ii) significant variation of the concentrations of reactants and structure-directing agents during synthesis, and (iii) lack of control over the rate and orientation of the crystallization process.

To advance toward the solution of the above problems, we present in this paper a new strategy for the synthesis of silicalite-1 in which two solutions of different concentration (that upon mixing give rise to the zeolite precursor gel) are initially separated by means of the above-mentioned laser-

* Corresponding author. E-mail: coronas@unizar.es.
[†] Department of Chemical and Environmental Engineering, University of Zaragoza.
[‡] Institute of Materials Science of Aragon, CSIC−University of Zaragoza.
[§] Department of Earth Sciences, University of Zaragoza.
[#] Nanoscience Institute of Aragon, University of Zaragoza.

(1) Corma, A.; Rey, F.; Rius, J.; Sabater, M. J.; Valencia, S. *Nature* **2004**, *431*, 287−290.
(2) Kuznicki, S. M.; Bell, V. A.; Nair, S.; Hillhouse, H. W.; Jacubinas, R. M.; Braunbarth, C. M.; Toby, B. H.; Tsapatsis, M. *Nature* **2001**, *412*, 720−724.
(3) Stankiewicz, A. *Chem. Eng. Proc.* **2003**, *42*, 137−144.
(4) Anastas, P. T.; Kirchhoff, M. M.; Williamson, T. C. *Appl. Catal., A* **2001**, *221*, 3−13.
(5) Jeong, H. K.; Krych, W.; Ramanan, H.; Nair, S.; Marand, E.; Tsapatsis, M. *Chem. Mater.* **2004**, *16*, 3838−3845.
(6) Davis, M. E. *Nature* **2002**, *417*, 813−821.
(7) Choi, J.; Ghosh, S.; Lai, Z.; Tsapatsis, M. *Angew. Chem., Int. Ed.* **2006**, *45*, 1154−1158.
(8) Coronas, J.; Santamaría, J. *Top. Catal.* **2004**, *29*, 29−44.
(9) Lai, S. M.; Ng, C. P.; Martin-Aranda, R.; Yeung, K. L. *Microporous Mesoporous Mater.* **2003**, *66*, 239−252.
(10) Vilaseca, M.; Coronas, J.; Cirera, A.; Cornet, A.; Morante, J. R.; Santamaría, J. *Catal. Today* **2003**, *82*, 179−185.
(11) Mintova, S.; Mo, S.; Bein, T. *Chem. Mater.* **2001**, *13*, 901−905.
(12) Moos, R.; Müller, R.; Plog, C.; Knezevic, A.; Leye, H.; Irion, E.; Braum, T.; Marquardt K. -J. Binder K. *Sens. Actuators, B* **2002**, *83*, 181−189.
(13) Cheng, X.; Wang, Z.; Yan, Y. *Electrochem. Solid-State Lett.* **2001**, *4*, B23−B26.
(14) McDonnell, A. M. P.; Beving, D.; Wang, A.; Chen, W.; Yan, Y. *Adv. Funct. Mater.* **2005**, *15*, 336−340.
(15) Nishiyama, N.; Ichioka, K.; Park, D. -H.; Egashira, Y.; Ueyama, K.; Gora, L.; Zhu, W.; Kapteijn, F.; Moulijn, J. A. *Ind. Eng. Chem. Res.* **2004**, *43*, 1211−1215.
(16) Valtchev, V.; Mintova, S. *Microporous Mesoporous Mater.* **2001**, *43*, 41−49.
(17) Matsufuji, T.; Nishiyama, N.; Matsukata, M.; Ueyama, K. *J. Membr. Sci.* **2000**, *178*, 25−34.
(18) Dong, A.; Wang, Y.; Tang, Y.; Ren, N.; Zhang, Y.; Gao, Z. *Chem. Mater.* **2002**, *14*, 3217−3219.
(19) Mateo, E.; Lahoz, R.; de la Fuente, G. F.; Paniagua, A.; Coronas, J.; Santamaría, J. *Chem. Mater.* **2004**, *16*, 4847−4850.

10.1021/cm062317p CCC: $37.00 
Published on Web 01/03/2007

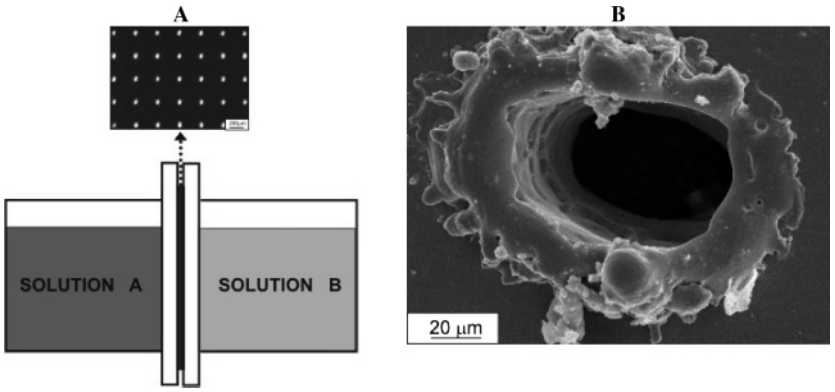


**Figure 1.** (A) Scheme of the synthesis of zeolites by the reactant separation method. (B) SEM image of a microhole with its rough edge in detail.

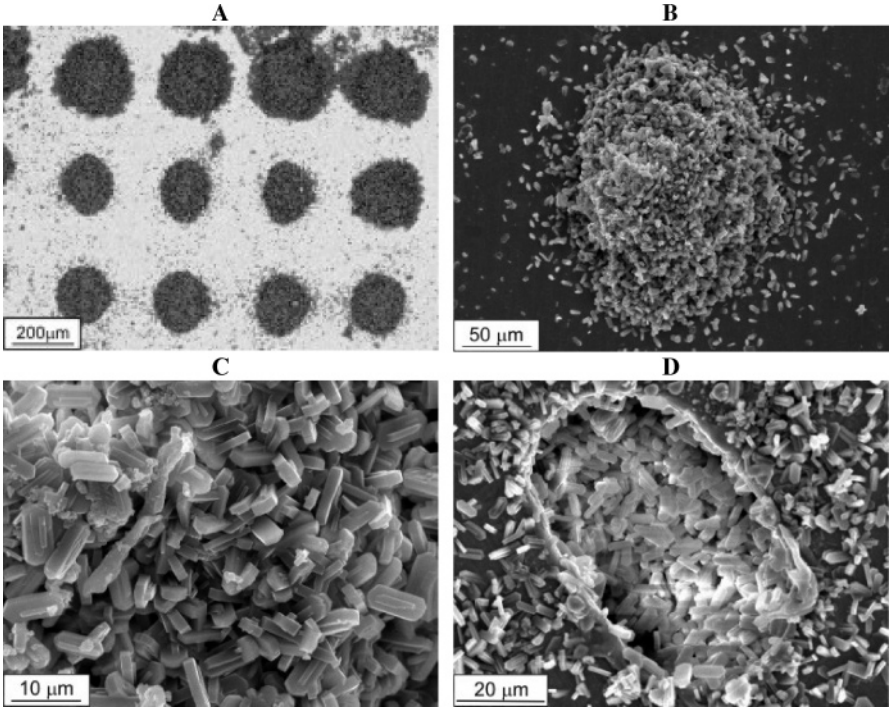


**Figure 2.** SEM images of a reactant separation experiment ($\epsilon = 1.8\%$) using solutions A1 and B1. (A) Back-scattering of the rough edge side in contact with solution A1. (B) Detail of (A). (C) Detail of (B). (D) The opposite side.

perforated stainless steel sheet. During the hydrothermal synthesis, because of concentration gradients, reactant diffusion from each side promotes crystallization of silicalite-1 in a controlled manner inside the microperforations. A scheme of this concept is presented in Figure 1a. This synthesis strategy allows for easy control of the growth of silicalite-1 inside the ca. 80 $\mu$m in diameter microperforations. In addition, the following advantages of this reactants separation method, when compared to the traditional systems employed for the preparation of zeolite films, may be highlighted: (i) the concentration of a given zeolite precursor can be separately varied in each side of the support, which is important for avoiding crystallization of the zeolite either in the homogeneous (liquid) phase or on the nondesired support surfaces, and hence to produce crystallization only inside the support pores; (ii) the hydrothermal synthesis is self-regulated, finishing when the zeolite layer is completed and both support sides become isolated; (iii) a preferential crystallographic orientation can be achieved in the growth of the zeolite inside the microperforations.

## Experimental Section

To perforate the 75 $\mu$m thick stainless steel sheets (5 Cr, 18 Ni, Record), we used a 65 W, Q-switched Nd:YAG laser manufactured by Baasel Lasertech, emitting at a wavelength of 1064 nm in both continuous and pulsed modes. Perforation was achieved via ablation of the steel substrate, performed at a surface scan rate of 1500 mm/s, an average power of 4 W, a pulse repetition rate of 4.5 kHz, a pulse energy of 0.80 mJ, a fluence of 1.3 MJ/mm$^2$, and an irradiance of 3.14 GW/mm$^2$. Microholes were patterned on stainless steel sheets to yield arrays of 1.8, 6.6, and 7.7% porosity ($\epsilon$), that is, approximately 643, 2651, and 3103 microholes/cm$^2$, respectively. The laser-drilled holes are inherently associated with the formation

**Table 1. Molar Compositions of A and B Solutions, Where TPAOH is Tetrapropylammonium Hydroxide and TEOS is Tetraethylorthosilicate**

| solution | molar composition |
|---|---|
| A1 | $TPAOH/H_2O = 1/50$ |
| B1 | $TEOS/H_2O = 1/50$ |
| A2 | $H_2O = 1$ |
| B2 | $TEOS/TPAOH/H_2O = 3.125/1/516$ |

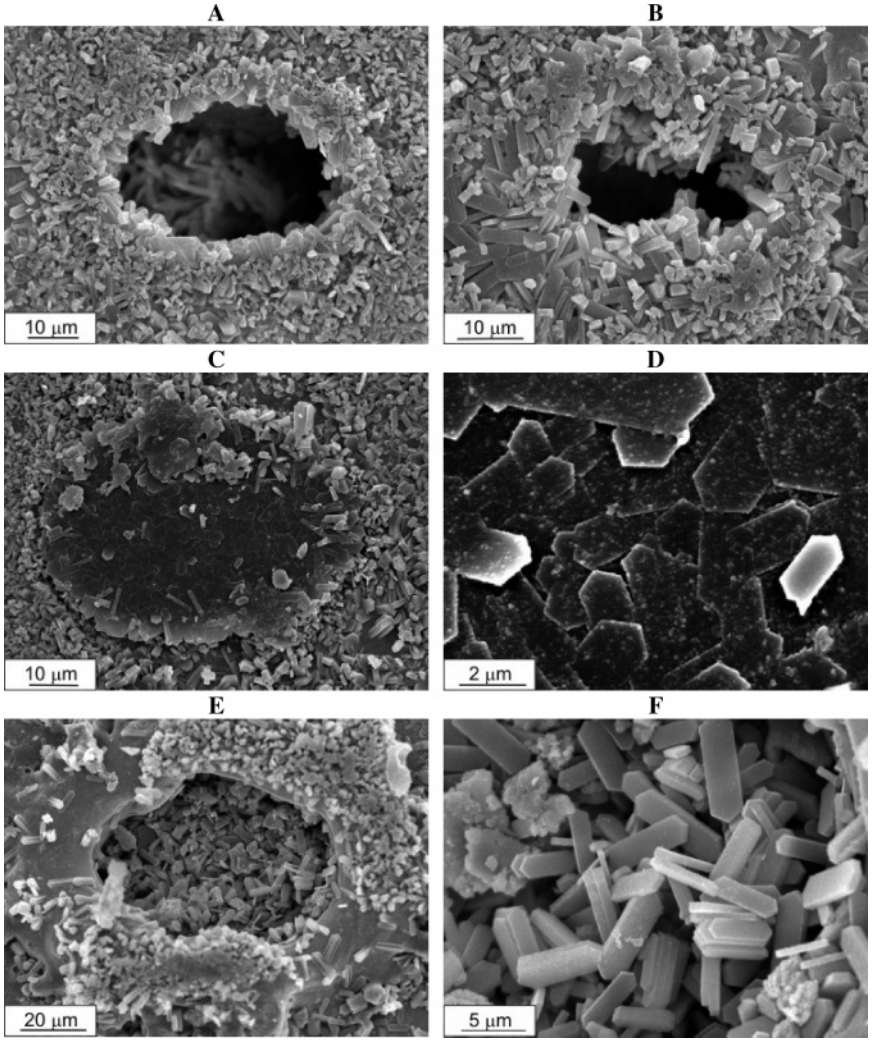


**Figure 3.** SEM images of a reactant separation experiment ($\epsilon = 7.7\%$) using solutions A2 and B2. (A−C) Three different views of the smooth side in contact with solution B2. (D) Detail of (C). (E) The opposite side. (F) Detail of (E).

of rough edges (Figure 1b) due to the expulsion of molten steel from their inside.[19]

A stainless steel Teflon-lined autoclave was designed ad hoc for applying the reactant separation method using a circular laser-perforated stainless steel sheet. The 15 or 20 mm diameter circular sheet was sealed in the middle of the autoclave by means of Teflon gaskets. Two stagnant, equal volume spaces were then produced: one was filled with solution A, the other with solution B. Table 1 shows the possible molar compositions of A and B solutions. Solution A was always in contact with the rough edge support side. The hydrothermal synthesis took place at 180 °C for 24 h, keeping the autoclave in a horizontal position and the perforated sheet vertical. Under these conditions, the silicalite-1 crystals were produced mostly within the microholes rather than on the outside support surface. Once the synthesis was finished, after being washed with deionized water and drying overnight at 100 °C, the sheets were calcined at 480 °C for 8 h, with heating and cooling rates of 0.5 °C/min. Having some similarity with the experimental system here, a polymer membrane was used to separate a seeded clear aluminosilicate solution and an amorphous aluminosilicate gel in the zeolite A synthesis,[20] whereas the hydrothermal synthesis of zeolites has been already carried out on metallic supports.[21,22]

## Results and Discussion

**Zeolitic Diaphragm.** Figure 2 shows the SEM (JEOL JSM-6400 operating at 20 kV) images of a reactant separation experiment in which solution A1 ($TPAOH/H_2O = 1/50$) was placed in contact with the rough edge side of the microperforated stainless steel sheet, whereas solution B1 ($TEOS/H_2O = 1/50$) was placed on the opposite side. These two solutions cannot yield by themselves the synthesis of zeolite silicalite-1, because each side contains necessary reactants. However, TPAOH diffuses from solution A1 to solution B1 and TEOS from solution B1 to solution A1. This process mainly favors the crystallization of the zeolite inside the microholes where the $[TEOS]/[TPAOH]/[H_2O]$ ratio reached is more adequate. To a certain extent, this is a self-regulating process, because a faster rate of crystallization is expected for the regions where the ratio is optimal. Even if some silicalite-1 crystals can be found (because interdiffusion is likely faster than crystallization under the conditions employed; actually, as ascertain by ICP analysis, at the end of the synthesis, the silicon concentration is the same at both sides) on the external surface of the stainless steel sheet,

(20) Bronic, J.; Subotic, Boris, B.; Skreblin, M. *Microporous Mesoporous Mater.* **1999**, *28*, 73−82.
(21) Kölsch, P.; Venzke, D.; Noack, M.; Toussaint P.; Caro, J. *J. Chem. Soc. Chem. Commun.* **1994**, 2491−2491.
(22) Kölsch, P.; Venzke, D.; Noack, M.; Lieske, E.; Toussaint, P.; Caro, J. *Stud. Surf. Sci. Catal.* **1994**, *84*, 1075−1082.

back-scattering SEM Figure 2a shows that most of the zeolite was synthesized inside the microhole and around its entrance. Figure 2b confirms this situation and, along with Figure 2c, shows in detail the typical MFI-type morphology of the zeolite crystals synthesized. Figure 2a−c corresponds to the rough edge side, whereas Figure 2d corresponds to the other side. These SEM images allow us to say that the microholes can be filled with zeolite crystals, minimizing the synthesis on both external surfaces of the perforated stainless steel sheet. Also, the laser treatment could have activated the inside of the microperforations for crystal growth, as it is sometimes difficult to grow a zeolite layer on a stainless steel support.[23] Note that when all the reactants are together, a thick layer is produced that covers the whole perforated sheet (where most of the surface support was not affected by the laser).[19]

Next, reactant separation experiments were performed by putting solution A2 ($H_2O$) in contact with the rough edge of the microperforated stainless steel sheet, whereas solution B2 (TEOS/TPAOH/$H_2O$ = 3.125/1/516) was in contact with the opposite side. This situation makes that TEOS and TPAOH diffuse from solution B2 to solution A2, which affects the distribution of crystals along the microholes, as will be shown next. On the other hand, as seen above, with the new method of synthesis proposed here, it is possible to promote the growth of silcalite-1 inside the microperforations of the stainless steel sheet. The laser ablation may activate the area for growth inside the microperforations. Hence, there should be a correlation between the porosity of the support (defined as the fraction of area occupied by the microholes) and the volumes of the precursor solutions of a given composition used to allow the crystallization of zeolite in all the microholes. In these experiments a high value of porosity (7.7%) was chosen so that the total amount of nutrients in the autoclave was defective when related to the area for growth. As a consequence, it is possible in only one experiment to partially fill some of the microholes (images A and B of Figure 3), whereas others are completely closed, with zeolite crystals that have grown with clear preferred crystallographic orientation (images C and D of Figure 3). If SEM images 3A−D are from the solution B2 side, SEM images E and F of Figure 3 are from solution A2 side, where the intergrowth between silicalite-1 particles is not evident. Figures 3A−C could be also considered as being different moments of the filling and closing of a microhole with silicalite-1 crystals, noting that the mouth of a certain microhole is being closed by means of a kind of imaginary diaphragm made of silicalite-1 crystals.

**Crystallographic Orientation Control.** The MFI-type structure of silicalite-1 has straight channels with a pore opening of 0.54 × 0.56 nm along its *b*-axis and sinusoidal channels of 0.51 × 0.55 nm along its *a*-axis. The characteristic crystal shape of silicalite-1 crystals is usually referred to as a coffin one.[24] The channels and typical shape of a silicalite-1 crystal are shown in Figure 4 (top). The crystals in the above-mentioned zeolitic diaphragm have mostly grown with their *b*-axes perpendicular to the support. In

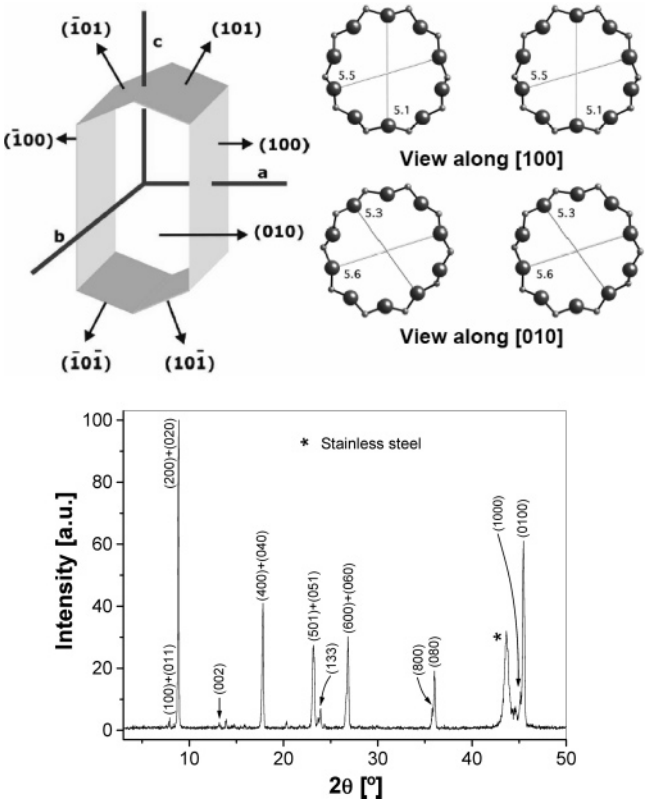


**Figure 4.** Top: Typical crystal shape and channels[25] of the MFI-type zeolite. Bottom: XRD analysis performed on the solution B2 side of a sample prepared in the same conditions used for sample in Figure 3.

agreement with this, Figure 4 (bottom) shows the XRD (Rigaku/Max diffractometer Cu Kα radiation and graphite monochromator) pattern of the material in the solution B2 side. The peak marked in Figure 4 (bottom) with an asterisk corresponds to the stainless steel support. The dominant peaks are (*h*00) and (0k0) ((200) and (020), (400) and (040), etc.), and there are always considerably minor (*h*00) peak intensities (when they can be distinguished from (0*k*0) peaks). At the same time, (002) and (133) peaks also have very small intensities. Consequently, most of the crystals are oriented with their *b*-axes perpendicular to the stainless steel support. To quantify the orientation degree, we calculated the CPO (crystallographic preferred orientation) index[26] using areas under the (200)+(020), (133), and (002) peaks

$$\mathrm{CPO}_{(200)+(020)}^{(133)} = \frac{\left(\frac{A_{(200)+(020)}}{A_{(133)}}\right)_S - \left(\frac{A_{(200)+(020)}}{A_{(133)}}\right)_P}{\left(\frac{A_{(200)+(020)}}{A_{(133)}}\right)_S}$$

$$\mathrm{CPO}_{(200)+(020)}^{(002)} = \frac{\left(\frac{A_{(200)+(020)}}{A_{(002)}}\right)_S - \left(\frac{A_{(200)+(020)}}{A_{(002)}}\right)_P}{\left(\frac{A_{(200)+(020)}}{A_{(002)}}\right)_S}$$

where *A* is the area under a given peak and S and P refer to the sample and reference powder, respectively. For the

(23) Valtchev, V.; Mintova, S. *Zeolites* **1995**, *15*, 171−175.
(24) Bonilla, G.; Díaz, I.; Tsapatsis, M.; Jeong, H. K.; Lee, Y.; Vlachos, D. G. *Chem. Mater.* **2004**, *16*, 5697−5705.
(25) Mintova, S.; Hedlund, J.; Valtchev, V.; Schoeman, B. J.; Sterte, J. *J. Mater. Chem.* **1998**, *8*, 2217−2221.

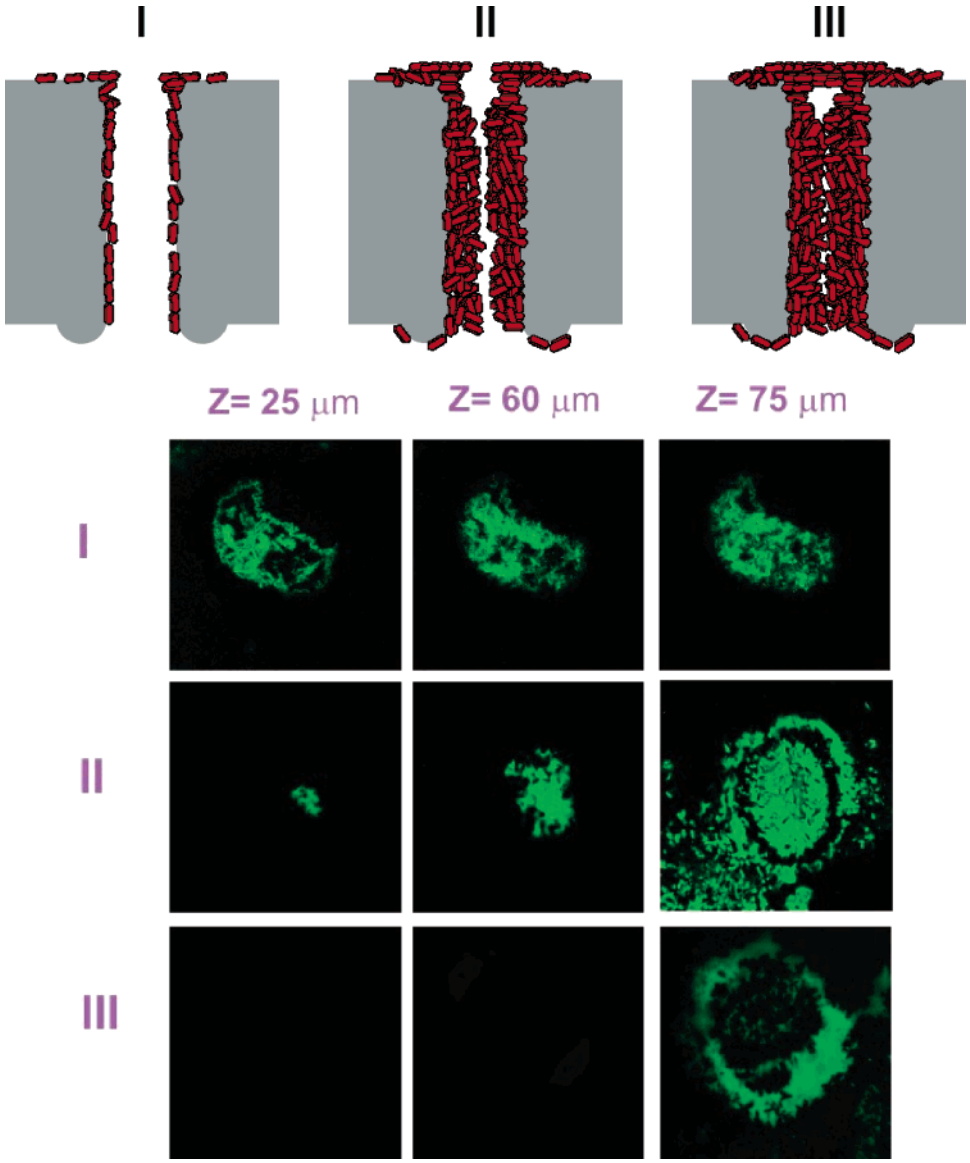


**Figure 5.** Top: Scheme of the mechanism proposed for the reactant separation silicalite-1 synthesis using solutions A2 and B2. Bottom: Fluorescence confocal microscopy performed on samples prepared in the same conditions used for sample in Figure 3: I, a nonclosed, nonfilled microhole; II a closed, almost-filled microhole; III, a closed, filled in most of its length microhole.

sample in Figure 4 (bottom), $CPO_{(200)+(020)/(133)}$ and $CPO_{(200)+(020)/(002)}$ were 0.94 and 0.92, respectively, close to unity, indicating strong *a* and *b* out-of-plane preferential orientations (basically preferential *b*-orientations, as said above) for the zeolitic material synthesized on the laser-drilled stainless steel sheets. $CPO_{(200)+(020)/(133)}$ and $CPO_{(200)+(020)/(002)}$ were calculated for nine samples prepared in the same conditions to obtain average values, followed by their standard deviations, of $0.94 \pm 0.07$ and $0.93 \pm 0.07$, respectively. This gives an idea of the reproducibility of the process.

**Mechanism of Crystallization.** The time evolution of the zeolitic diaphragm inferred from Figure 3A−C suggests a crystallization of silicalite-1 in the microholes represented in three different moments in Figure 5 (top). Initially, the nucleation of the zeolite is only possible in the solution B2 ($TEOS/TPAOH/H_2O = 3.125/1/516$) side, whereas the diffusion of TPAOH and TEOS nutrients to solution A2 ($H_2O$) takes place simultaneously, driven by the concentration gradient. This diffusion process should favor the transport of silicalite-1 nuclei, produced in solution B2, into the microholes, mostly to be deposited on their inner surface. This transport of nuclei is also responsible for the fact that some silicalite-1 crystals are found in the water side at the end of the synthesis. Small silicalite-1 particles deposited or synthesized on the mouths of the microholes in contact with solution B2 make the crystallization process faster there, and *b*-oriented silicalite-1 crystals begin to produce a sort of zeolitic diaphragm that gradually reduces its opening and therefore the communication between both support sides. Note that the silicalite-1 crystals constituting the zeolitic diaphragm grow perpendicularly to the pore mouth surface, as in the case of *c* out-of-plane preferred orientation

(26) Baerlocher, C.; Meier W. M.; Olson, D. H. *Atlas of Zeolite Framework Types*; Elsevier: Amsterdam, 2001.

(27) Lai, Z.; Bonilla, G.; Díaz, I.; Nery, J. G.; Sujaoti, K.; Amat, M. A.; Kokkoli, E.; Terasaki, O.; Thompson, R. W.; Tsapatsis, M.; Vlachos, D. G. *Science* **2003**, *300*, 456−460.

membranes prepared by secondary growth.[27] Following the diaphragm evolution, the microperforations (or a large number of them) are eventually blocked by the crystallizing zeolite and the diffusion process stops. Crystallization may still proceed, however, using whatever nutrients are available at each side. As a result, microholes are covered with continuous, closed zeolitic diaphragms (images c and d of Figure 3), only a few micrometers thick, whereas their inner volumes could be only partially filled with zeolite crystals.

The mechanism described above was confirmed by further analysis carried out by fluorescence confocal optical microscopy (Leica SP2, using an Ar laser emitting at 488 nm), using a fluorochrome molecule (2′,7′-difluorescein) as dye. This technique allows one to scan many thin sections through the near cylindrical microperforations to build a three-dimensional image of the sample. Also, in the case of thick (up to 25 $\mu$m) polycrystalline MFI-type membranes, the mechanism was demonstrated by combining simultaneous reflectance and fluorescence imaging with SEM to show the fluorescent features that correspond to grain boundaries.[28] Here, sections of three different pores with an appearance similar to those in Figure 3A−C, obtained at the same depths of 25, 60, and 75 $\mu$m from the stainless surface in contact with solution B2, are presented in Figure 5 (bottom). Because the stainless steel sheets used here are 75 $\mu$m thick, we are evaluating the presence of empty spaces through most of the pore length (which could not be observed by SEM), shown in green. Adequately excited, the selected fluorochrome emits green light. Microscopy images in Figure 5 (bottom, I) belong to a nonclosed, nonfilled zeolite pore, as the green color can be found at any chosen section in the 25−75 $\mu$m range of the pore length. Note that the section is more elliptical when compared to that of an as-drilled microhole (Figure 1b) because of the growth of silicalite-1 in the pore walls. Figure 5 (bottom, II) shows different sections of a closed, almost-filled zeolite pore. Because the pore is closed, having a similar appearance to that shown in Figure 3c, the confocal microscopy allows a closer examination of the zeolitic diaphragm, showing in this case that the microhole is not completely filled. It seems that there is a central channel (revealed by the higher intensity of the green color in the middle of the sections) that probably has been conducting reactants from each side (as if it were a stalactite) until the last moment, when the pore closed. Figure 5 (bottom, III) depicts a closed, filled in most of its length microhole where the fluorochrome scarcely emits.

## Conclusion

The use of a laser-microperforated, 75 $\mu$m thick stainless steel sheet allows the implementation of a new method for the hydrothermal synthesis of zeolites (silicalite-1): the method of separation of reactants, which works by introducing solutions of different concentration (that when mixed give rise to a common zeolite precursor gel) into each side of the sheet. The concentration gradients established at the beginning of the process drive the diffusion of reactants from each side, promoting crystallization of silicalite-1 crystals on each microperforation of the stainless steel sheet. By adjusting the concentrations in each side, we can obtain b-oriented films. Finally, this strategy could be applied to prepare micromembranes or to coat the inner surface of a microperforation.

**Acknowledgment.** Financial support from DGA and MEC (PPQ2003-04986, MAT2004-02184, and CGL2004-05055/BTE projects), both in Spain, is gratefully acknowledged, and also the Precision Mechanical Service of the University of Zaragoza.

CM062317P

(28) Snyder, M. A.; Lai, Z.; Tsapatsis, M.; Vlachos, D. G. *Microporous Mesoporous Mater.* **2004**, *76*, 29−33.